Selenium effects on prostate cell growth

Article *in* Cancer Epidemiology Biomarkers & Prevention · December 2000

Source: PubMed

3 authors, including:

David G Menter
University of Texas MD Anderson Cancer Center
184 PUBLICATIONS **5,661** CITATIONS
SEE PROFILE

Scott Lippman
University of California, San Diego
780 PUBLICATIONS **62,853** CITATIONS
SEE PROFILE

Selenium Effects on Prostate Cell Growth[1]

David G. Menter, Anita L. Sabichi, and Scott M. Lippman[2]

Department of Clinical Cancer Prevention, The University of Texas M. D. Anderson Cancer Center, Houston, Texas 77030 [D. G. M., A. L. S., S. M. L.], and Cancer Control Research Committee, Southwest Oncology Group, San Antonio, Texas 78245 [A. L. S., S. M. L.]

Abstract

Epidemiological and clinical data suggest that selenium may prevent prostate cancer, but the biological effects of selenium on normal or malignant prostate cells are not well known. We evaluated the effects of sodium selenite (Na_2SeO_3) or *l*-selenomethionine (SeMet) on monolayer and anchorage-independent growth in a series of normal primary prostate cultures (epithelial, stromal, and smooth muscle) and prostate cancer cell lines (LNCaP, PC-3, and DU145). We observed differential, dose-dependent growth inhibition and apoptosis within prostate cancer cells (compared with normal prostate cells) treated with 1–500 μM of Na_2SeO_3 or SeMet. Na_2SeO_3 more potently inhibited growth at any given concentration. The androgen-responsive LNCaP cells were the most sensitive to selenium growth suppression (IC_{50}s at 72 h for Na_2SeO_3 and SeMet were 0.2 and 1.0 μM, respectively). Growth of the primary prostate cells virtually was not suppressed (IC_{50}s at 72 h for Na_2SeO_3 and SeMet were 22–38 and >500 μM, respectively). We also observed that DNA condensation and DNA fragmentation (terminal deoxynucleotidyltransferase dUTP nicked- end labeling/fluorescence-activated cell sorting) were elevated in selenium-treated cells and that activated caspase-3 colocalized with terminal deoxynucleotidyltransferase dUTP nick end labeling-stained cells by immunofluorescence. Higher basal poly(ADP-ribose) polymerase (PARP) expression levels and PARP cleavage (a substrate for caspase-3) were observed during apoptosis in tumor cells, compared with normal cells. Selective tumor cell death was associated with an increase in sub-G_0-G_1 cells after propidium iodide staining and fluorescence-activated cell sorting analysis. SeMet caused an increase in arrest in the G_2-M phase of the cell cycle selectively in cancer cells. Inhibition of cancer cell growth by SeMet was associated with phosphorylation of P-Tyr15-p34/cdc2, which caused growth arrest in the G_2-M phase. Anchorage-independent growth of prostate cancer cells in soft agar was sensitive to selenium. Our results suggest that Na_2SeO_3 is the more potent inducer of apoptosis in normal and cancer prostate cells. Our SeMet results involving PARP and G_2-M cell-cycle arrest (cited above) indicate that SeMet selectively induces apoptosis in cancer but not primary cells of the human prostate. Our overall findings are relevant to the molecular mechanisms of selenium actions on prostate carcinogenesis and help demonstrate the selective, dose-dependent effects of selenium (especially SeMet) on prostate cancer cell death and growth inhibition.

Introduction

Selenium is one of the most exciting and promising agents currently under laboratory and translational development for prostate cancer chemoprevention. Secondary clinical findings of Clark *et al.* (1, 2) are primarily responsible for generating the great interest in this agent. Clark *et al.* (1, 2) conducted a double-blind, placebo-controlled trial of selenium to prevent basal cell or squamous cell skin carcinoma in 1312 subjects (including 974 men) with a history of nonmelanoma skin cancer. Although negative regarding the primary skin cancer end point, the trial produced the strikingly positive secondary finding that prostate cancer incidence was reduced by 63% among men in the selenium arm (*versus* in the placebo arm). This finding is supported by epidemiological data (3) and prompted our present laboratory study of the *in vitro* biological effects of selenium on normal human prostate cells and human prostate cancer cells.

For the past decade, prostate cancer has been second only to nonmelanoma skin cancer as the most commonly diagnosed cancer in American men. Lifetime risks for prostate cancer are 16.6 and 18.1% for Caucasian and African-American men, respectively (4). Therefore, the public health implications of identifying an effective chemopreventive agent against this disease are tremendous.

Although well established as an essential micronutrient of animal and human diets, the activity of selenium in human prostate carcinogenesis is only just beginning to undergo evaluation. Selenium is an essential element in redox pathways and has been identified as one of the many dietary factors with the potential to modify carcinogenesis (5–8). This element is widely distributed in soil, forages, and grains (9). It is present in plants in both inorganic (*e.g.*, selenite and selenate) and organic (*e.g.*, selenocysteine and selenomethionine) forms (10). Organic forms of selenium such as SeMet[3] are more bioavail-

Received 6/6/00; revised 8/31/00; accepted 9/12/00.
The costs of publication of this article were defrayed in part by the payment of page charges. This article must therefore be hereby marked *advertisement* in accordance with 18 U.S.C. Section 1734 solely to indicate this fact.
[1] This work was supported by Grants 5U10CA37429 and CA16672 from the National Cancer Institute, NIH, and TPRN-99-240-01-CNE-1 from the American Cancer Society. S. M. L. holds the Margaret and Ben Love Professorship in Clinical Cancer Care.
[2] To whom requests for reprints should be addressed, at Department of Clinical Cancer Prevention, The University of Texas M. D. Anderson Cancer Center, 1515 Holcombe Boulevard, Box 236, Houston, TX 77030. Phone: (713) 745-3672; Fax: (713) 794-4679; E-mail: slippman@mdanderson.org.

[3] The abbreviations used are: SeMet, *l*-selenomethionine; Na_2SeO_3, sodium selenite; PrEC, prostate epithelial cell; PrSM, prostate smooth muscle; PrSt, prostate stromal; DAPI, 4,6-diamidino-2-phenylindole dihydrochloride; TUNEL, terminal deoxynucleotidyltransferase dUTP nick end labeling; FACS, fluorescence-activated cell sorter; CMF, calcium- and magnesium-free; PARP, poly(ADP-ribose) polymerase; PI, propidium iodide; IC_{50}, inhibitory concentration of 50% growth; MSC, methylselenocysteine.

able than are inorganic forms such as Na_2SeO_3 (11). The metabolism and bioavailability are influenced by absorption in the gastrointestinal tract, transport in the blood, metabolism and storage in tissues, and excretion rate in the urine and feces (11).

In the present study, we examined selenium effects on the growth, cell cycle, and apoptosis of prostate cancer cells and normal prostate cells. We evaluated the effects of both an inorganic selenium (Na_2SeO_3) and organic selenium (SeMet) in primary tissue culture. We used both androgen-responsive (LNCaP) and androgen-unresponsive (PC-3 and DU145) cancer cells. The normal cell types were PrECs, PrSM cells, and PrSt cells. To our knowledge, this is the first report of a comparative *in vitro* analysis of the apoptosis and growth arrest effects of selenium in a comprehensive panel of human prostate cancer and normal cells.

Materials and Methods

Prostate Cells and Culture Conditions

Primary cultures of normal human prostate cells PrEC, PrSt, and PrSM were purchased from Clonetics (San Diego, CA). These primary cell cultures were maintained in defined culture medium (Clonetics) and passaged using trypsin-EDTA (Clonetics) according to the manufacturer's instructions. The LNCaP cell line was isolated from a lymph node, PC-3 cell line from a bone metastasis, and DU145 cell line from a brain metastasis of prostate cancer patients. These cells were maintained in DMEM and F-12 (mixed 1:1) medium supplemented with 10% fetal bovine serum and passaged using trypsin-EDTA.

Growth Inhibition Assay

Cells were plated into 96-well tissue culture plates and allowed to establish monolayers overnight. Either Na_2SeO_3 or SeMet in various concentrations was added to chosen wells and grown for 24, 48, or 72 h. The assay was terminated by washing cells with PBS and then fixing them with 1% paraformaldehyde in PBS. Fixed cells were washed and stained with 0.2% crystal violet in 50 mM 3-(cyclohexylamino)-1-propanesulfonic acid buffer at pH 9.5 for 30 min. Plates were washed, allowed to dry, and then solubilized using 10% glacial acetic acid. Samples were analyzed by using a Biolumin 960 microtiter plate reader (Molecular Dynamics, San Diego, CA) at an absorption wavelength of 590 nm and normalized based on control well absorbency. These data were then reduced to growth inhibition percentages in relationship to untreated control samples. The inhibitory concentration of 50% growth (IC_{50}) was determined using a Statview statistics program (SAS Institute, Inc., Cary, NC) by using a logically weighted least squares regression algorithm called Lowess at a tension parameter setting of 66. Independent experiments were performed using trypan blue exclusion. Cells were evaluated by light microscopy on a hemocytometer to determine viability, and these experiments provided comparable results.

Apoptosis Assays

DNA Condensation Assay. Cells were grown in 24-well plates and treated with various concentrations of Na_2SeO_3 or SeMet. Cells were harvested using 0.25% trypsin, 2 mM EDTA in PBS, resuspended in ~100 μl of Cytofix, and stored in an Eppendorf tube at 4°C. After placing cells in Cytofunnel, they were spun onto coated Cytoslides at 750 rpm in a Cytospin 2 centrifuge (Shandon, Pittsburgh, PA). Cells were postfixed with 4% paraformaldehyde in PBS for 1 h at 25°C and permeabilized for 10 min with 1% Triton X-100 in 0.1 M citrate buffer (pH 6.0). Samples were washed with PBS and stained with either DAPI or Hoechst 33258 stain (Molecular Probes, Eugene, OR) at a final concentration of 1.0 μM overnight at 4°C, washed in distilled H_2O, and mounted in Prolong antifade solution (Molecular Probes). Slides were analyzed by light microscopy, and data were acquired using digital image analysis. Our image analysis system uses a Quantix air-cooled, black and white CCD camera (Photometrics, Tucson, AZ) that is driven by IPlabs software (Scanalytics, Inc., Fairfax, VA) using a Macintosh G3 computer (Apple Computer, Cupertino, CA). This image acquisition equipment is attached to an IX70 inverted research light microscope equipped with epi-illumination objectives (Olympus America, Inc., Lake Success, NY).

TUNEL Assay. Laminin was adsorbed to 12-mm round coverslips by incubating for 1 h at 25°C in 24-well tissue culture plates at a concentration equivalent to 1 $\mu g/cm^2$. After washing, cells were plated on laminin-coated coverslips 24 h prior to exposure to selenium compounds. After treatment, the coverslips were washed with PBS and fixed with 1% paraformaldehyde in PBS. Coverslips were washed again with PBS, and the cells were permeabilized with 1% Triton X-100 in 0.1 M citrate buffer at pH 6.0. Cells were then incubated with an Apotag (Roche, Indianapolis, IN) enzymatic reaction mixture containing terminal deoxynucleotidyl transferase and FITC-dUTP according to the manufacturer's instructions, with slight modification. Coverslips were inverted on top of 30 μl of reaction mixture on parafilm that had been placed over #1 Whatman paper moistened with distilled H_2O lying on the bottom of a glass baking tray. After covering the tray with a plastic cover, it was placed in a humidified incubator, and the reaction was performed at 37°C for 90 min. Coverslips were washed by dipping 10 times in a beaker containing 1 liter of distilled H_2O. They were then mounted on glass slides using Prolong antifade solution (Molecular Probes). This method was also used to stain the Cytoslides described above. Slides were analyzed by light microscopy, and data were acquired and analyzed on our digital image acquisition system.

A similar TUNEL method was used to analyze samples by FACS. The APO-DIRECT system (Phoenix Flow Systems, Inc., San Diego, CA) was used for FACS analysis according to the manufacturer's instructions with slight modification. Floating cells that had been grown on 10-cm dishes and treated with the different selenium compounds were harvested by washing monolayers with CMF-PBS. The cells in wash buffer were centrifuged at 300 $\times$ *g* for 5 min at 4°C and placed on ice. The monolayers were trypsinized for 10 min in PBS containing 2 mM EDTA and 0.25% trypsin. These samples were pooled and resuspended in 1% paraformaldehyde in PBS and fixed for 15 min on ice. Samples were centrifuged at 800 $\times$ *g* for 5 min and resuspended in PBS containing 1% Triton X-100 and incubated on ice for 10 min. Cells were washed with PBS followed by centrifugation, resuspended in 70% ethanol, and stored at −20°C until analyzed with the APO-DIRECT protocol according to the manufacturer's instructions.

Immunofluorescent and Morphological Assessment of Apoptosis. Cells grown on coverslips using methods described above were also stained to detect caspase-3 activation or P-Tyr15-p34/cdc2 (New England Biolabs). Samples were blocked with Superblock (Pierce Chemical Co., Rockford, IL) solution in Tris-buffered saline (TBS) containing 0.1% Tween 20 (Pierce Chemical Co.). Primary rabbit polyclonal antibodies that recognize either the activated caspase-3 or P-Tyr15-p34/cdc2 were diluted in this Superblock solution and incubated in

24-well tissue culture dishes overnight at 4°C. Samples were rinsed two times with PBS and incubated with Texas Red-X goat antirabbit secondary antibody or Alexa 488 goat antirabbit secondary antibody (Molecular Probes). Samples were rinsed three times in PBS and one time in distilled H_2O and mounted on glass slides using Prolong antifade mounting medium (Molecular Probes). Slides were then analyzed by epi-fluorescence microscopy, and data were acquired using digital image analysis.

After staining cells on coverslips with primary and secondary antibodies, we counterstained cells with DAPI to identify the nuclear DNA and Alexa-594-phalloidin (Molecular Probes) to identify cytoplasmic actin. Cells were counterstained with 500 nM DAPI stain and 1 unit/ml Alexa-594-phalloidin in Superblock solution containing 0.1% Tween 20 overnight at 4°C. Samples were rinsed three times in PBS and one time in distilled H_2O and mounted on glass slides using Prolong antifade solution (Molecular Probes). Slides were then analyzed by light microscopy, and data were acquired using digital image analysis.

Western Analysis

Cell monolayers were washed twice with cold CMF-PBS and removed from tissue culture plates by scraping into cold CMF-PBS on ice. Samples were then pelleted at 12,000 $\times$ *g* and solubilized. The packed cells were solubilized 3:1 (v/v) in solubilization buffer to cells in a buffer solution containing 1% NP40, 1 mM $NaMoO_4$, 30 mM NaF, 1 mM EDTA, 1 mM $NaVO_4$, 30 mM Tris (pH 8.3), 100 mM NaCl, and Complete protease inhibitor cocktail (Roche). Protein levels were determined using the Bradford protein assay on a Biolumin 960 (Molecular Dynamics, San Diego, CA) microtiter plate reader. Proteins were separated on Bis-Tris 4–12% polyacrylamide gradient electrophoresis gels and electrotransferred using the NuPage system (Novex, San Diego, CA) to 0.45-μm nitrocellulose membranes (Schleicher and Schuell, Keene, NH). Membranes were blocked with 3% bovine serum albumin in TBS with 1% Tween 20 (TBST) and incubated with primary antibodies at 4°C in the same blocking solution. After washing three times in TBST, blots were incubated with the suitable horseradish peroxidase-conjugated secondary antibodies (Pierce Chemical Co.) and washed again three times. SuperSignal West (Pierce Chemical Co.) chemiluminescence detection procedures were followed according to the manufacturer's instructions. Blots were exposed to Hyperfilm (Amersham, Arlington Heights, IL), followed by development in a Kodak automatic film processor (Eastman Kodak, Rochester, NY). Western data were digitized on a laser scanning densitometer (Molecular Dynamics, San Diego, CA) and quantified using NIH image version 1.62. Data were analyzed for statistical significance using Statview (SAS Institute, Inc., Cary, NC).

Soft Agar Colony Formation Assay

An agarose feeder layer was prepared by combining 12 ml of 2$\times$ DMEM with 6 ml of 1.8% melted agar that was cooled to just above 37°C, and the mixture was placed into six-well plates after the addition of various concentrations of selenium compound. After the feeder layer solidified, a low percentage agar layer was prepared by combining 5 ml of cells in DMEM/F-12 and 10% fetal bovine serum with 1 ml of 1.8% melted agar. The DU145 cells were plated at 1500 cells per well, and the LNCaP or PC-3 cells were plated at 2000 cells per well. The final mix of cells, medium, and agar was cooled to just above 37°C and selenium compound was added in the same concentrations as in the feeder layer. Cells were placed in a humidified incubator and fed periodically with a fresh agar-selenium mixture. Colonies were evaluated at 2 weeks using bright-field illumination through a $\times$1.25 lens on an IX70 inverted microscope (Olympus). Data were digitized using a Quantix CCD camera (Photometrics) and analyzed using IPlabs software (Scanalytics).

Results

Selenium Effects on Cell Growth. Fig. 1 and Table 1 illustrate the concentration-dependent and time-dependent effects of both Na_2SeO_3 and SeMet. Na_2SeO_3 and SeMet were each given in concentrations ranging from 1–500 μM. The growth of prostate cancer cells LNCaP, PC-3, and DU145 was inhibited at lower IC_{50} concentrations by both Na_2SeO_3 and SeMet at 72 h than was the growth of normal prostate cells PrEC, PrSM, and PrSt (Table 1). Over the experimental time course, we observed a significant suppression of tumor cell growth compared with normal cells (Fig. 1). Na_2SeO_3 was consistently a more potent growth inhibitor than SeMet (Table 1). Generally, PrECs were least effected by increasing concentrations of Na_2SeO_3 and SeMet (Fig. 1). The strongest growth inhibiting activity of Na_2SeO_3 or SeMet was in androgen-responsive LNCaP cells. Na_2SeO_3 at IC_{50} concentrations between 0.2 and 3.9 μM was a potent growth inhibitor of all prostate cancer cells at 72 h compared with an effective IC_{50} concentration range of 22–38 μM in primary prostate cells. SeMet treatment demonstrated the greatest differential IC_{50} between prostate carcinoma cells (1–90 μM) and normal prostate cells ($>$500 μM) at 72 h, suggesting that SeMet more selectively inhibited growth of prostate cancer cells, compared with normal cells (Table 1).

Analysis of Cell Death. Normal and malignant prostate cell lines were examined for evidence of apoptosis after exposure to 1–500 μM of Na_2SeO_3 or SeMet. We present apoptosis data based primarily on 10 μM of Na_2SeO3 and 500 μM of SeMet at 48 h, which were the best conditions for presenting side-by-side comparisons between tumor and normal cells. These conditions also were necessary experimentally, because there was a tendency of the LNCaP cells to lift off the tissue culture substrata at longer times or higher concentrations.

Selenocompounds induced less apoptosis in normal prostate cells compared with tumor cells when we initially examined cells grown on laminin-coated coverslips or Cytoslides using fluorescence microscopy. In these initial experiments, apoptosis was examined by triple staining coverslips or double staining Cytoslides containing untreated cells and those treated with either Na_2SeO_3 or SeMet (Fig. 2*A*). Coverslips were triple stained (Fig. 2*A*) using the FITC-dUTP TUNEL method (*inset* with *green* stain, outlined in *white*), counterstained with DAPI (*blue* stain) to study DNA condensation, and then immunostained for activated caspase-3 (*inset* with *red* stain, outlined in *white*). Cytoslides (Fig. 2*A*) were double stained with FITC-dUTP TUNEL method (*insets* with *green* stain, outlined in *yellow*) then counterstained with DAPI (*inset* with *blue* stain, outlined in *yellow*). Control samples demonstrated little evidence of apoptosis shown in Cytospin samples by FITC-dUTP-TUNEL (Fig. 2*A*, *inset* with *green* stain, outlined in *yellow*). Few selenium-treated normal cells stained for FITC-dUTP, condensed DAPI, and activated caspase-3 (Fig. 2*A*). In contrast, selenocompounds induced high levels of apoptosis in prostate carcinoma cells, demonstrated by nuclear DNA condensation that colocalized with FITC-dUTP and activated capase-3 (Fig. 2*A*). These staining patterns were most prevalent in the Na_2SeO_3-treated cells when compared with the SeMet-treated

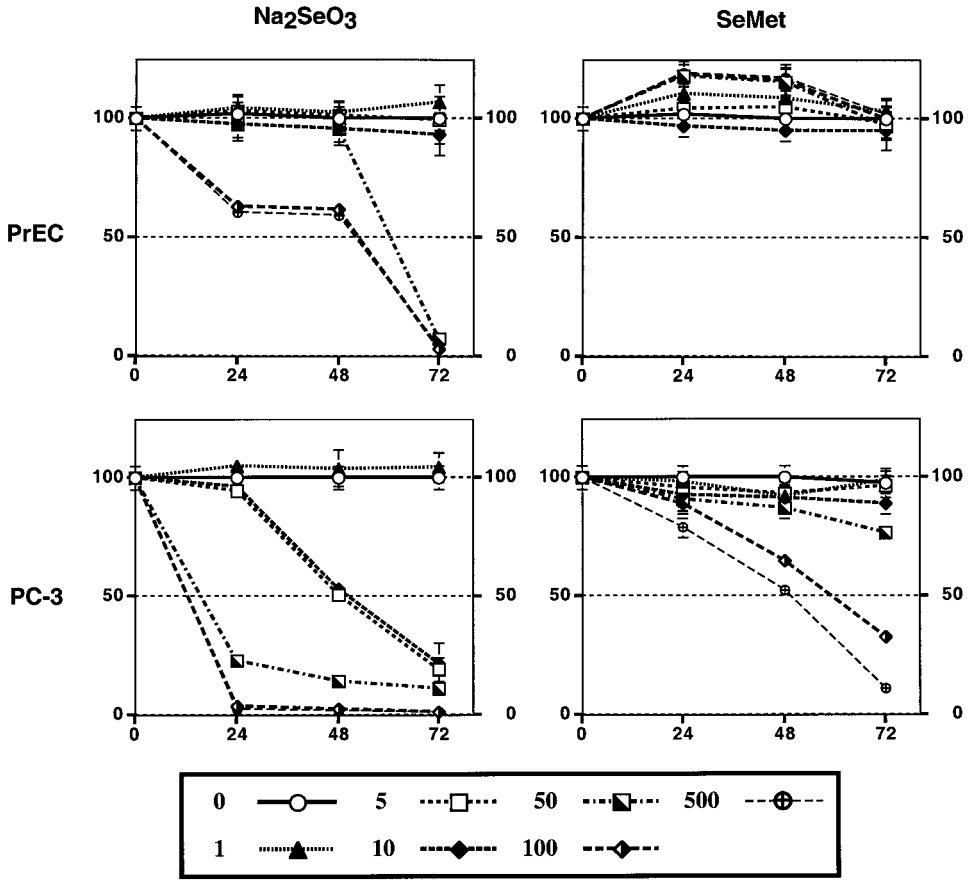

Fig. 1. Prostate cells were treated with two selenium compounds, inorganic Na_2SeO_3 or organo-*l*-SeMet, at a concentration range of 1–500 μM. The growth of normal PrECs was compared with the growth of prostate cancer cells (androgen-unresponsive PC-3) at 24, 48, and 72 h (*X axis*). The *Y axis* indicates cell growth in percentages. Note the dose-dependent growth suppression by both Na_2SeO_3 and SeMet. The data are represented as the means of six measurements of each concentration level after normalization to untreated control samples; *bars*, SD.

Table 1 IC_{50}[a]

Cell type	Experimental condition					
	Na_2SeO_3			SeMet		
	24 h	48 h	72 h	24 h	48 h	72 h
PrEC	>500	>500	27	>500	>500	>500
PrSM	85	20	38	>500	>500	>500
PrSt	58	20	22	>500	>500	>500
LNCaP	4.8	5	0.2	170	130	1
PC-3	15	12	3.7	>500	>500	70
DU145	70	70	3.9	>500	>500	90

[a] IC_{50}s in μM.

samples, although SeMet caused a significant difference in staining of tumor cells in contrast with normal (Fig. 2*A*).

We quantified the DNA condensation by analyzing digital images of DAPI- or Hoechst-stained Cytospin samples (Fig. 2*B*). Many cells detached from laminin-coated substrata as they began to die. We collected the nonadherent cells and the remaining adherent cells after EDTA-trypsin harvesting and combined these two cell subpopulations. DNA condensation was observed within 48 h in prostate cells after Na_2SeO_3 as well as after SeMet treatment (Fig. 2*B*). The androgen-responsive LNCaP carcinoma cells exhibited the highest level of DNA condensation after selenium treatment, followed by PC-3 and DU145 cells, in order of sensitivity (Fig. 2*B*). Selenium-treated PrECs exhibited between 7.5- and 23-fold less DNA condensation compared with tumor cells (Fig. 2*B*). Selenium-treated PrSM and PrSt cells exhibited between 4.7- and 5.3-fold more DNA condensation than PrECs but 1.9–3.8-fold less DNA condensation than tumor cells (Fig. 2*B*).

We quantified the DNA fragmentation that occurred during apoptosis using TUNEL-FACS analysis. We collected and pooled the nonadherent cells and the remaining monolayer cells as described above. TUNEL-FACS analysis demonstrated FITC-dUTP incorporation into the DNA of Na_2SeO_3 as well as SeMet-treated dying cells (Fig. 2*C*). The androgen-responsive LNCaP cells exhibited the highest level of nicked-end DNA labeling after treatment with both selenium compounds. The PC-3 cells were also sensitive to selenium treatments, followed by DU145 cells (Fig. 2*C*). SeMet- and Na_2SeO_3-treated PrEC

and PrSt cells did not exhibit significant levels of DNA fragmentation, whereas PrSM exhibited ~25% fragmentation with Na_2SeO_3.

Selective Promotion of PARP Cleavage by Selenium. PARP is a substrate of the caspase-3 protease during apoptosis; therefore, we examined cell lysates for PARP cleavage after selenium treatment by Western analysis (Fig. 2*D*). There were substantial differences observed in PARP expression between normal cells and tumor cells. The intact PARP molecule migrates at M_r 116,000, and the antibody (clone 4C10-5) we used recognizes the intact M_r 116,000 molecule and two cleavage products, M_r 85,000 and M_r 48,000 subfragments. We observed a profound difference for basal PARP expression of the intact M_r 116,000 molecule in normal prostate cells compared with tumor cells (Fig. 2*D*). The untreated PrECs, PrSM cells, and PrSt cells did not express the intact PARP molecule when grown to ~80% confluence (Fig. 2*D*, *column 1*), whereas tumor cell lines expressed distinct baseline levels (Fig. 2*D*, *columns 2* and *3*). These findings may reflect the ability of normal cells to undergo contact inhibition.

PARP cleavage in Na_2SeO_3-treated tumor cells was complete with no intact M_r 116,000 PARP observed at the earliest 24-h treatment point. A M_r 85,000 cleavage product appeared within 24 h in the LNCaP, PC-3, and DU145 cells (Fig. 2*D*, *column 2*). In comparison, the cleavage of PARP in the SeMet-treated cells gradually occurred over the full time course (Fig. 2*D*, *column 3*). In the SeMet-treated DU145 cells, the predominant cleavage fragment was a M_r 48,000 form, whereas in the other cells, the predominant cleavage product was the M_r 85,000 form. This variation in cleavage fragment profiles may reflect heterogeneity of the cleavage sites for the multiple forms of caspases that result in a context-specific or cell-specific proteolytic processing mechanism (12). Whether the various cleavage fragments exert different effects on a given cell population remains to be determined.

Cell Cycle Analysis of Selenium-treated Prostate Cells. PI staining of cellular DNA, followed by FACS analysis, provides a useful method for evaluating the cell cycle (Fig. 3*A*). We observed PI staining of apoptotic cells at sub-G_0-G_1 levels of the cell cycle that corresponded to TUNEL-FACS data. The SeMet-treated normal prostate cells did not exhibit the same extent of sub-G_0-G_1 subpopulation cells as did the prostatic carcinoma cells (Fig. 3, *A* and *B*). Androgen-responsive LNCaP cells (Fig. 3, *A, column 2,* and *B*) exhibited the highest total increase in sub-G_0-G_1 cell fraction of any line examined after treatment with Na_2SeO_3 (23.1%) or SeMet (41.5%). We also observed an increase in sub-G_0-G_1 cells after Na_2SeO_3 of 13.5% in PC-3 cells or 14.7% in DU145 cells. Similarly, sub-G_0-G_1 cells after SeMet treatment of either PC-3 cells or DU145 cells increased 12.1 or 11.2% (Fig. 3, *A* and *B*).

A higher percentage of untreated PrECs were in the G_2 phase of the cell cycle compared with untreated tumor cells (Fig. 3, *A, column 1,* and *C*). Greater than 20% of the PrECs and PrSM cells were in the G_2 phase, which most likely reflects contact inhibition typical of normal cells. Treatment of both normal and tumor cells with Na_2SeO_3 resulted in a smaller change in the G_2 subfraction in PrEC (3%), PrSM (−3%), and PrSt (2%) cells as opposed to LNCaP (6%), PC-3 (4%), and DU145 (12%) tumor cells. SeMet treatment selectively increased the percentage of the G_2 subfraction cancer cells compared with normal cells (Fig. 3*C*). When we examined the percentage increase in G_2 cell cycle phase cells after SeMet treatment, there was a modest 8% increase in PrECs, 4% increase in PrSM cells, and a 1% increase in PrSt cells. In contrast, SeMet caused a significant increases in G_2 cells (Fig. 3*C*), particularly in LNCaP (13%), PC-3 (32%), and DU145 (20%) cells.

We also assessed the selenium effects on percentages of cells in S-phase. In PrEC cells, Na_2SeO_3 produced a 3% increase and SeMet a 12% increase in S-phase cells. In PrSM cells, Na_2SeO_3 and SeMet produced increased S-phase cells by 11 and 6%, respectively. In PrSt cells, Na_2SeO_3 and SeMet produced increased S-phase cells by 12 and 6%, respectively. In LNCaP tumor cells, we observed little change in S-phase after Na_2SeO_3 (3% increase) or SeMet (5% decrease). In contrast, treating the PC-3 cells and DU145 cells with Na_2SeO_3 increased their respective S-phase components by 28 and 26%, whereas SeMet treatment caused <2% increases.

Phosphorylation of cdc2 on Tyr15 Coincides with G_2 Cell Cycle Arrest. The phosphorylation of cdc2 on Tyr15 by WEE1 and MIK protein kinases causes cells to arrest in the G_2-M transition phase of the cell cycle (13, 14). To determine whether the accumulation of cells in the G_2-M phase observed by PI-FACS is associated with phosphorylation of cdc2 on Tyr15, we examined cells by immunofluorescence. We used optimized concentrations of Na_2SeO_3 (10 μM) and SeMet (500 μM) for cell cycle studies. Treatment of all cells with Na_2SeO_3 caused an increase in nuclei labeled with anti-phospho-cdc2 (Tyr15) antibody. Tumor cells demonstrated observable increases in P-Tyr15-p34/cdc2 after SeMet treatment that were not apparent in the normal cells (Fig. 4*A*). When we examined nuclei using DAPI counterstaining, the P-Tyr15-p34/cdc2 colocalized mainly with the nuclei. In some instances, there also was some perinuclear staining that was observed in some of the SeMet-treated PC-3 samples (Fig. 4*A*, *white arrows*), which also occurred in the DU145 (data not shown). When we examined cellular morphology using Alexa-594-conjugated phalloidin as a counterstain that labels actin microfilaments, we observed differential effects on cytoskeletal structures that depended on which compound was used, Na_2SeO_3 or SeMet. The Na_2SeO_3 treatment caused the disadherence of both normal and tumor cells that was preceded by rounding up of the cells. PC3 cells (Fig. 4*A*, *yellow bracket*) and DU145 cells (data not shown) specifically formed numerous spike-shaped actin filament bundles in response to Na_2SeO_3 treatment. In contrast, SeMet treatment primarily caused tumor cells to either round-up and detach or spread out their cytoskeleton. The most intense P-Tyr15-p34/cdc2 staining appeared to associate with the nuclei of cells that had rounded-up.

The percentage of P-Tyr15-p34/cdc2-containing cells relative to DAPI-stained nuclei was determined by counting using digital capture and image analysis (Fig. 4*B*). Normal PrECs exhibited little phosphorylation of P-Tyr15-p34/cdc2, whereas PrSM and PrST exhibited a more extensive presence of phosphoprotein in the Na_2SeO_3-treated samples. All of the selenium-treated LNCaP cells that remained attached to laminin substrata exhibited P-Tyr15-p34/cdc2 label. A high proportion of the selenium-treated PC-3 and DU145 cells that remained attached were positive for P-Tyr15-p34/cdc2 (Fig. 4*B*).

To confirm that cdc2 was phosphorylated on Tyr15, we examined detergent-solubilized cell lysates after selenium treatment for 6 and 48 h by Western analysis. After SeMet treatment, Cdc2 phosphorylation ranged from 75 to 127% higher at 6 h in tumor cells compared with 2–15% higher at 6 h in normal cells by densitometry. In epithelial cells, there was only a 0.4% increase in cdc2 phosphorylation after treatment with Na_2SeO_3 (Fig. 4*C*, *Lane 2*) and 2.4% increase with SeMet-(Fig. 4*C*, *Lane 3*) treated samples. There was a low level of P-Tyr15-p34/cdc2

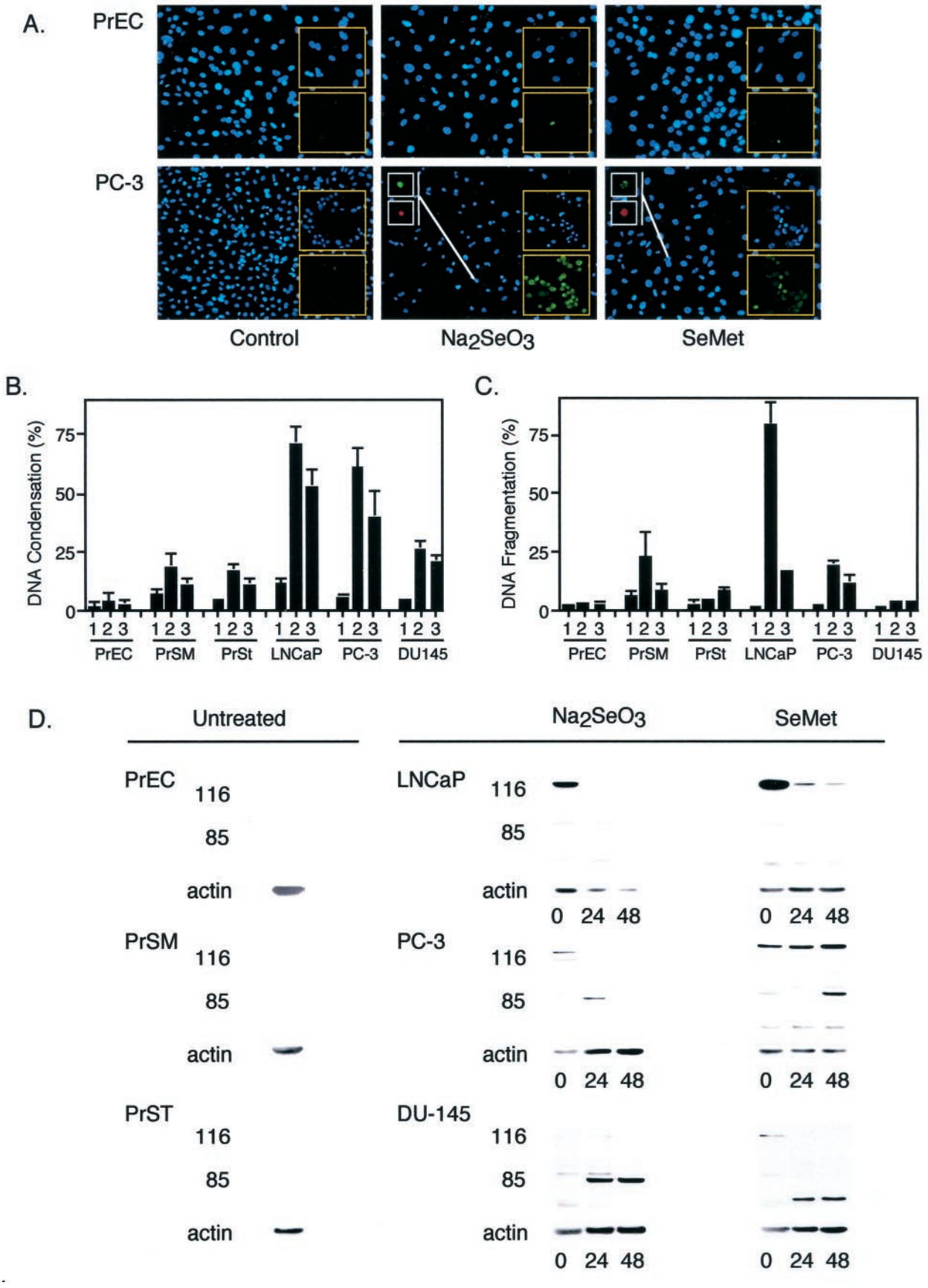
A.
PrEC
PC-3
Control
Na2SeO3
SeMet
B.
DNA Condensation (%)
75
50
25
0
1 2 3
PrEC
PrSM
PrSt
LNCaP
PC-3
DU145
C.
DNA Fragmentation (%)
D.
Untreated
Na2SeO3
SeMet
PrEC
PrSM
PrST
LNCaP
PC-3
DU-145
116
85
actin
0 24 48

in the untreated tumor cells at the 6 and 48 h (*Lane 1*). There was a statistically significant increase in P-Tyr15-p34/cdc2 phosphoprotein formation in tumor cells after treatment with Na_2SeO_3 at 6 h ($P < .0001$) that was reduced at 48 h, most likely reflecting the loss of viable cells because of increased apoptosis (Fig. 4*C*, *Lane 2*). There was a significant increase in P-Tyr15-p34/cdc2 in all of the tumor cells after 6 h of SeMet treatment ($P < 0.0001$) that remained higher than controls through 48 h (Fig. 4*C*, *Lane 3*). These data are consistent with the increase in G_2-M-phase tumor cells observed using PI-FACS (Fig. 3*C*) and the immunostaining of adherent cells (Fig. 4*A*). Taken together, these data support the notion that G_2-M cell-cycle arrest of tumor cells after SeMet treatment involves cdc2-Tyr15 phosphorylation.

Selenium Effects on Prostate Cancer Cell Colonies in Soft Agar. We also examined the number and size distribution of tumor colonies that formed in soft agar in the presence of selenium compounds. Computerized imaging and segmentation analyses were performed to determine the colony number and average colony size. SeMet inhibits the number of colonies formed from single cell clones (Fig. 5). Selenium compounds profoundly affected the size distribution of colonies that grew in soft agar, reflecting the clonal growth or expansion rate of each colony. The size and number of LNCaP, PC-3, and DU145 prostate cell colonies were decreased in the presence of organic SeMet in all cancer cell lines (Fig. 5). Tumor cell colony size and number were also inhibited by treatment with Na_2SeO_3 (data not shown).

Discussion

Our present *in vitro* study provides direct support and rationale for selenium as a prostate cancer prevention agent. Our major findings are: (*a*) selenium has differential effects in prostate cancer *versus* normal cells; (*b*) selenium-induced growth inhibition and apoptosis in cancer cells are dose-dependent; and (*c*) selenium has greater activity in androgen-sensitive (LNCaP) *versus* androgen-insensitive (PC-3 and DU145) cancer cells. We present the first report of differential *in vitro* effects of selenium on growth inhibition and apoptosis in a comprehensive panel of human prostate cancer and normal cells. Our major result of differential selenium-induced growth inhibition, apoptosis, and cell cycle arrest in prostate cancer (but not normal) cells is consistent with the earlier positive selenium epidemiological and clinical findings.

The biology of selenium, including toxic chemical effects, has been studied extensively in other cell systems. Many biological effects of selenium supplementation involve incorporation of selenocysteine into proteins such as SeGPX and thioredoxin reductase via selenocysteine insertion sequences (15–17). Although selenium primarily functions after insertion into the active sites of enzymes, it also can exhibit certain chemical activity independent of protein incorporation. Chemical activity ranges from direct oxidation of nucleotides, proteins, and cofactors (18, 19) to chemically altering the binding interactions between retinoids and the nuclear retinoic acid receptors (20). Profound chemical effects, however, generally were observed in studies involving inorganic forms of selenium at high concentrations. Shen *et al.* (18) found that 10 μM of Na_2SeO_3 induced apoptosis in HepG2 cells because of generation of reactive oxygen species.

Consistent with our findings, certain reports show extensive toxicity of Na_2SeO_3 on both normal and tumor cells but little effect of SeMet on normal cells. A study of a series of selenocompounds showed that Na_2SeO_3 and selenocystamine were the most potent agents in reducing glutathione and DNA damage, leading to apoptosis in normal mouse keratinocytes (21). SeMet had no significant chemical effects on normal mouse keratinocytes. Kajander *et al.* (22) also examined the *in vitro* cytotoxicity of SeMet and Na_2SeO_3 in a large panel of leukemia, lymphoma, and hepatoma cells, along with CHO, BHK, and normal fibroblasts. In this study (22), the selenium IC_{50} concentrations observed in the tumor cells (30–135 μM) were similar to ours (Table 1), but the normal fibroblasts IC_{50} concentrations were lower (160 μM). However, the normal fibroblasts required a much longer time period (10 days) than tumor cells (3 days) to reach 50% cell death. Redman *et al.* (23) demonstrated recently the *in vitro* inhibition of growth and induction of apoptosis in DU145 cells after SeMet treatment, which produced lesser such effects in normal diploid fibroblasts. Consistent with our findings (Table 1), they observed very high IC_{50} levels in treating normal fibroblasts (1 mM), compared with micromolar IC_{50} levels in treating cancer cells (23). These and our studies demonstrate a differential effect of SeMet at lower concentrations and shorter times to induce death in tumor cells compared with normal cells.

Understanding the biological activity of selenium is complicated by the variety of available dietary forms of selenium and by the dynamics of selenium metabolism. In addition to SeMet and Na_2SeO_3, other selenocompounds, *e.g.*, monomethylated selenium, may have chemopreventive activity (8, 24). Ip *et al.* (25) have reported that monomethylated selenium compounds can cause growth inhibition and apoptosis in rat mammary gland and epithelial cells *in vivo*. SeMet and other selenium compounds are dynamically metabolized into a wide array of products, and these derivatives may directly influence the chemopreventive effects of selenium (8, 24). The different metabolic pathways of SeMet and Na_2SeO_3 both produce H_2Se, which, after activation to selenophosphate, is a source of selenium for synthesis into selenoproteins (8, 24). H_2Se also can be further metabolized (for excretion) by a series of methylation reactions that generate additional reactive selenium species with potential chemopreventive properties (8, 24).

Other studies have reported differential rates of DNA fragmentation in the three prostate cancer cell lines that are consistent with our observations describing TUNEL-FACS. Analysis of DNA fragmentation has been a useful method for analyzing apoptosis. Tang *et al.* (26) performed an extensive apoptosis and DNA fragmentation analysis on human prostate cells after serum removal. The rank order of overall survivability of cells from lowest to highest was benign prostate hyperplasia, normal human prostate cells, LNCaP, PC-3, primary carcinoma, and DU145 cells. This ranking coincided with DNA fragmentation

Fig. 2. Selenocompounds induced less apoptosis in normal prostate cells (compared with prostate cancer cells). *A*, apoptosis was examined by triple staining for TUNEL (*green*), DNA condensation associated with apoptosis (*blue*), and activated caspase-3 (*red*; see text for details). *B* and *C*: *column 1*, untreated; *column 2*, Na_2SeO_3; *column 3*, SeMet. *B*, Cytospin samples consisted of pooled subpopulations of adherent and floating cells (*yellow-outlined insets*) and were quantified using computerized image analysis. *C*, adherent and floating cell subpopulations were pooled and stained using the APO-DIRECT TUNEL flow cytometry kit. *D*, cleavage of cellular PARP as an endogenous enzymatic target of caspase-3 was examined in whole-cell detergent lysates (30 μg/lane). Significant differences were observed between normal prostate cells and tumor cells in basal PARP protein expression levels. The intact PARP molecule migrates at M_r 116,000, whereas the major cleavage products recognized by the monoclonal antibody migrate at M_r 48,000 and M_r 85,000 fragments. Actin levels demonstrate the uniformity of protein loading between treated and untreated sample lanes.

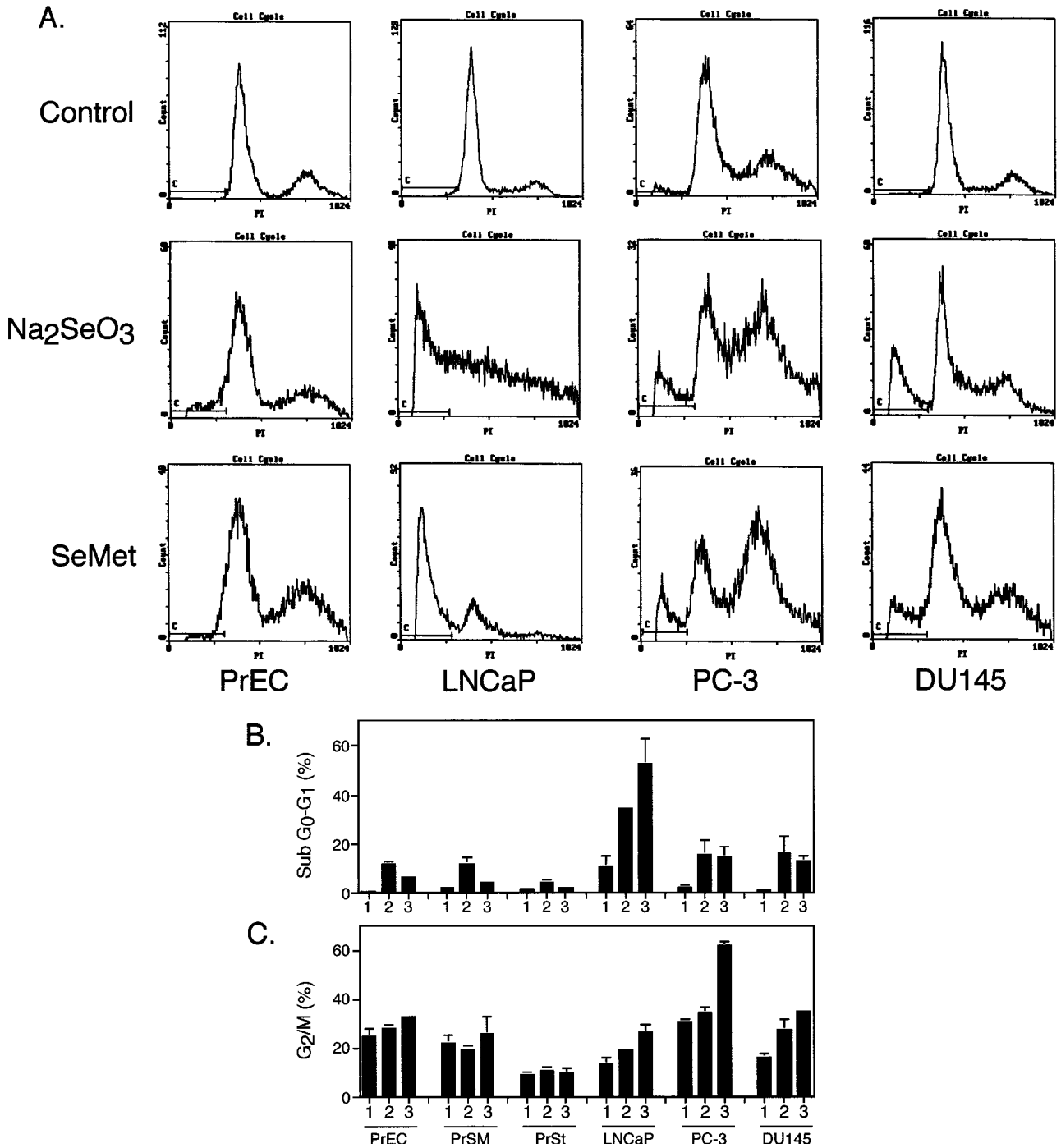

Fig. 3. Cell cycle analysis using PI intercalation into DNA was performed simultaneously with TUNEL-FACS assays. *A*, *columns 1–4*, representative examples of cell cycle profiles of PrEC, LNCaP, PC-3, and DU145 cells. Cells that occur at sub-G_0-G_1 levels of the cell cycle represent dead or dying cells (designated by *line C* at the base of the FACS profile). *B*, the sub-G_0-G_1 determinations are represented in this graph. *C*, a separate cell cycle analysis was performed on these data to determine cells in G_2-M arrest. SeMet caused significant increases in G_2-M phase cancer cells when compared with G_2-M arrested normal cells. *Bars*, SD.

profiles (26). The onset of apoptosis and the DNA fragmentation of the cell began to increase at day 2 in both the LNCaP and PC3 cells but were more gradual and protracted in the DU145 cells (26). These data are consistent with our observations of nicked-DNA formation by TUNEL-FACS (Fig. 2, *B* and *C*).

Many studies have examined the proteolysis of PARP by caspase-3 to demonstrate apoptotic activity. Our observations that PARP cleavage profiles are substantially different between prostate tumor and normal cells emphasize the selective nature of selenium effects on inducing tumor cell apoptosis (Fig. 2*D*). There are a growing number of biological properties attributed to PARP function that are coming under debate. PARP has zinc-finger DNA

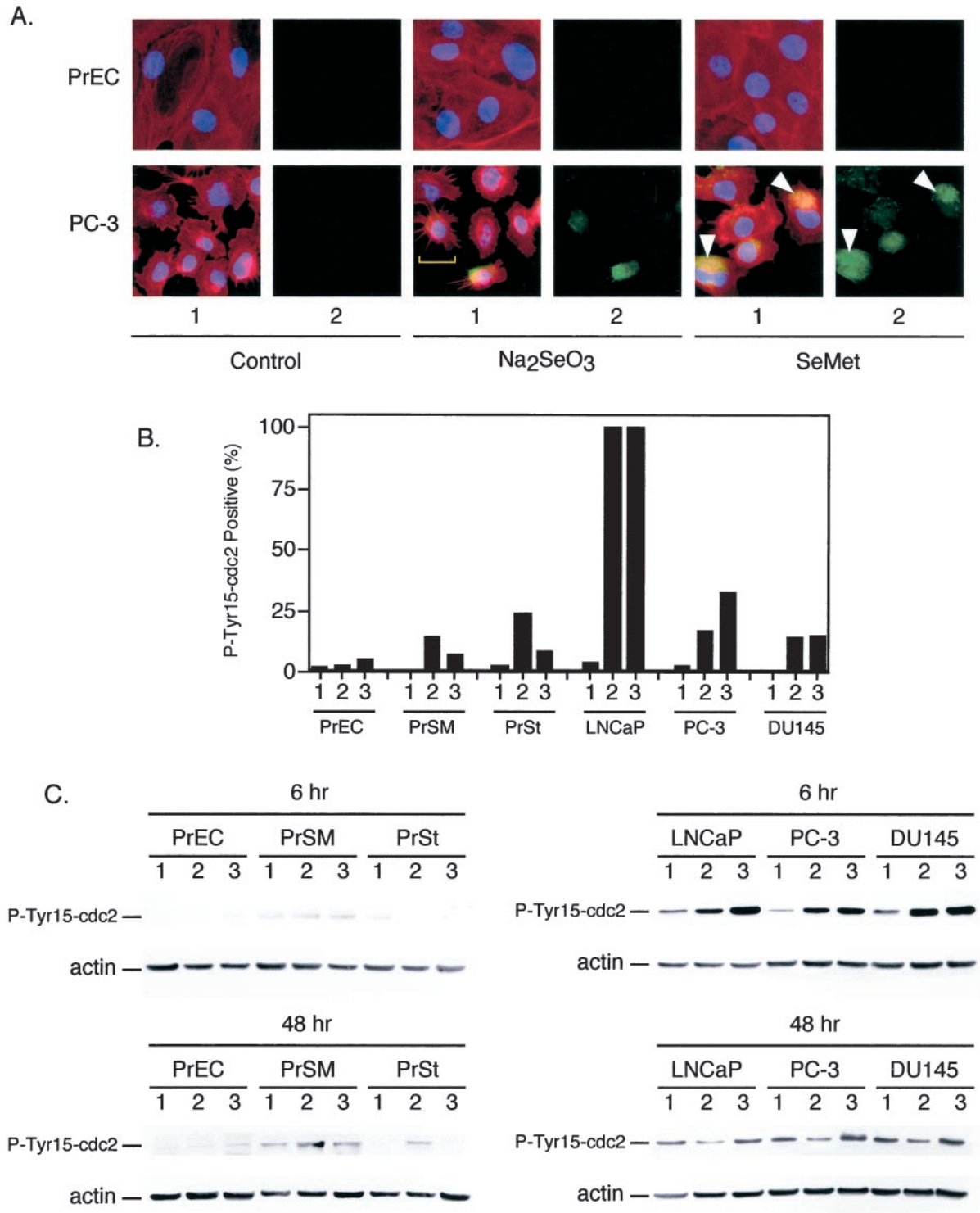

Fig. 4. Cell lines were examined for P-Tyr15-p34/cdc2 labeling by immunostaining cells attached to laminin-coated coverslips. *A*, samples were immunostained for P-Tyr15-p34/cdc2 [*green panels* in *column 2* of each treatment (*Control*, Na_2SeO_3, or *SeMet*)]. Samples were counterstained with DAPI to identify nuclei (*blue, column 1* of each treatment) and Alexa 594 conjugated phalloidin, which binds specifically to actin filaments (*red, column 1*). Data were merged to make a composite image (triple staining: *blue*, DAPI; *red*, actin; *green*, P-Tyr15-p34/cdc2) in each *column 1* (each *column 2* depicts P-Tyr15-p34/cdc2 data alone). The P-Tyr15-p34/cdc2-labeled areas are *white* to *yellow* in color where data were coincident (*column 1*). Intense *green* areas in the general images define data that were not coincidentally merged. Na_2SeO_3-treated PC-3 cells exhibit distinct actin processes (*yellow bracket*). SeMet-treated PC-3 cells exhibit cytoplasmic P-Tyr15-p34/cdc2-labeling (*white arrows*). *B*, the number of P-Tyr15-p34/cdc2-labeled cells was determined by counting Alexa 488 labeling (average of two experiments). *C*, selective cdc2 phosphorylation of tumor cells on Tyr15 was examined by immunoblot analysis. *B* and *C*: *1*, untreated; *2*, Na_2SeO_3; *3*, SeMet. Actin levels demonstrate the uniformity of protein loading between treated and untreated sample lanes.

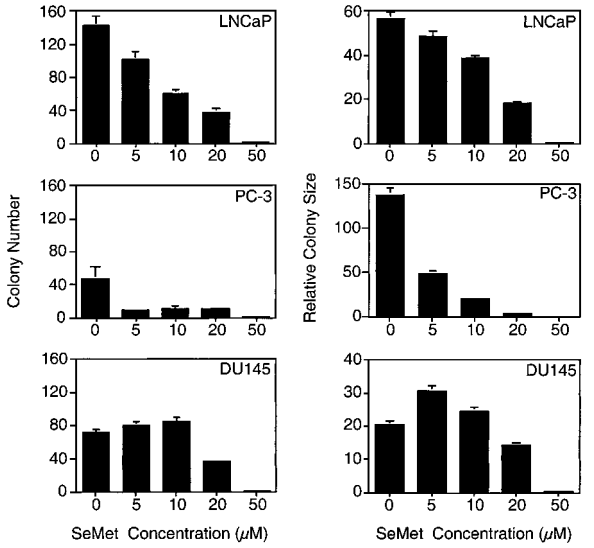

Fig. 5. The effect of selenium treatment on growth in soft agar was examined to evaluate the drug effects on anchorage-independent growth. Once the image is digitally acquired, the IPLabs program is used to perform segmentation and colony-size analysis. The data demonstrate the effect of selenium in inhibiting the numbers of total colonies formed from single-cell clones (*left column*) and colony size in pixels × 1000 (*right column*). These data were represented as the means of observations on three wells of a six-well plate; *bars*, SD. Two independent experiments were performed and provided similar results.

binding properties that enable the protein to detect and signal the occurrence of DNA strand breaks (27). PARP becomes enzymatically active when bound to DNA lesions. When its enzymatic activity is high, PARP converts nicotinamide dinucleotide to nicotinamide that can deplete ATP stores in the cell (28). The result of PARP activation is increased poly-ADP ribosylation of numerous nuclear proteins, including PARP itself. PARP activation occurs in response to genotoxic agents, such as alkylating agents and γ-irradiation. Another important PARP activity is to bind directly to retinoid X receptors and repress retinoid X receptor ligand-dependent transcriptional activities.

An important finding of the current report suggests that there may be a profound difference in PARP expression between contact-inhibited cells and cancer cells. The baseline expression of PARP in normal prostate cells was undetectable when we examined 30 μg of total protein from whole-cell lysates (Fig. 2*D*). Our findings are consistent with studies of PARP gene expression *in vivo* during prostate involution (29). PARP expression was virtually undetectable in rat ventral prostates, when examined after castration, which caused the involution of prostatic tissue (29). PARP expression increased over the next 4 days in association with apoptotic cell death (29). Prostate tissue mRNA samples were examined by Northern blot analysis to demonstrate a time-dependent increase in PARP that occurred during prostate involution (29). The pattern of PARP expression was confirmed by *in situ* hybridization. PARP expression was isolated to just a few epithelial cells in the control animals and increased dramatically in the epithelium and surrounding stromal tissues as prostatic involution progressed (29). The time frame for production of an M_r 85,000 subfragment after Na_2SeO_3 treatment was between 24 and 48 h in PrSM and PrSt cells (data not shown). Even with such dramatic increases in the M_r 85,000 proteins during these time periods, there continued to be very little intact M_r 116,000 PARP. These findings suggest that PARP production was induced because of apoptotic stress in contact-inhibited normal cells. Our findings further suggest that when PARP is produced, most of any intact molecules are rapidly degraded to inactive subfragments to minimize the effects of the intact molecule in contact-inhibited cells. These findings may be related to transient burst activity causing polyadenosinediphosphate-ribosylation of nuclear proteins as well after transients in PARP cleavage by caspase-3 (30–32). Selenium may exert its effects on this pathway through the selenoprotein, thioredoxin reductase, also described independently as a gene associated with retinoid-IFN-induced mortality (33). On the basis of these findings, it seems likely that thioredoxin reductase may induce caspase-3 activity in cancer cells. If selenium supplementation causes an increase in thioredoxin reductase in prostate cells, this may help explain the increase in caspase-3 activity (34).

In contrast with the absence of baseline PARP expression in normal cells, we found substantial baseline PARP levels in all three prostate tumor cell lines (Fig. 2*D, columns 2* and *3*). Uncleaved PARP expression was the highest in androgen-responsive LNCaP cells and was associated with the greatest sensitivity to both Na_2SeO_3 and SeMet treatment (Fig. 2*D*). The PC-3 and DU145 cells also expressed higher baseline levels of PARP and responded to both Na_2SeO_3 and SeMet treatment to a greater degree than did normal prostate cells. The differences in basal PARP expression may help explain why normal cells are more resistant to selenium-induced apoptosis than tumor cells. Because the tumor cells express higher basal levels of M_r 116,000 protein, even the slightest elevation of caspase-3 activity may lead to the cleavage of available PARP. This may lead to more rapid elimination of DNA repair capacity, making the tumor cells more sensitive to selenium treatment (35). These findings suggest the importance of PARP expression in the differential responses of normal prostate cells and prostate cancer cells to selenium.

Cell cycle analysis using DNA binding dyes often helps determine the status of cell populations in either growth fractions, growth arrest, or apoptosis (36). Dying cells accumulate in the sub-G_0-G_1 fraction of the cell cycle as they undergo apoptosis (36). These fractions represent cells that are dead or dying, including fragmented cell nuclei or apoptotic debris (37). We observed a selective increase in the sub-G_0-G_1 fraction of tumor cells compared with normal cells after Na_2SeO_3 or SeMet treatment (Fig. 3, *A* and *B*). The sub-G_0-G_1 fraction cell cycle profiles correlate with TUNEL-FACS labeling. The sub-G_0-G_1 fraction is underestimated by the computer because of debris from cell death (Fig. 3A, column 2). Cells that form decreased fluorescence subfraction, like those that we observed, have been shown previously to consist of apoptotic cells by ultrastructural analysis (37).

Cell cycle arrest at the G_2-M transition phase is one control mechanism that cells exert on proliferation. Apparently, G_2-M arrest protects cells from the lethality that results from undergoing cell division before repairing DNA damage (14). Eliminating cell growth by halting progression through the G_2-M transition state can also be caused by cell-cell contact inhibition as cells reach confluency (38). We observed many cells that were arrested in the G_2-M phase of the cell cycle (Fig. 3, *A* and *C*). There were many PrECs and PrSM normal cells arrested in the G_2-M cell cycle that associated with cell contact-induced growth inhibition (38). There was only a slight increase in normal cells at the G_2-M cell cycle checkpoint when they were treated with Na_2SeO_3 or SeMet (Fig. 3*C*). In contrast, there was an increase in tumor cells in the G_2-M phase after treatment with selenium, particularly when using SeMet (Fig. 3, *A* and *C*). Cells arrested at the G_2-M cell cycle

checkpoint doubled in all three tumor cell lines compared with a <10% increase in all of the normal cells.

Growth arrest in the G_2-M transition phase of the cell cycle has many important potential causes and outcomes. Reactive oxygen species, for example, can produce free radicals that promote cells to arrest in G_2-M (39). Free radicals can induce DNA and protein damage that activate protective mechanisms, resulting in growth arrest. Radiation damage is an important area of therapeutic intervention that relies on the generation of free radicals to induce macromolecular damage in cells. Studies have shown that G_2-M-arrested cells exhibit an increased sensitivity to ionizing radiation (40). When human prostatic carcinoma cell lines were examined using low-dose radiation exposure, there was a certain degree of variability in radiation sensitivity that depended on the cell line examined. The PC-3 cells that exhibited the most substantial increase in G_2-M-arrested cells was also the most sensitive to low-dose ionizing radiation. It is interesting to speculate that SeMet treatment may selectively enhance the radiosensitivity of prostatic carcinoma cells.

Growth control mechanisms rely heavily on phosphorylation or dephosphorylation of specific cell cycle molecules. cdc2 forms a complex with cyclin B1 during the G_2-M phase that controls cell mitosis (41). The phosphorylation status of cdc2 controls the progression of cells through the G_2-M phase of the cell cycle. Growth arrest at the G_2-M cell cycle phase is mediated by phosphorylation of cdc2 on Tyr15 and threonine 14 by WEE1 and MIK protein kinases (13, 14). The progression through G_2 into mitosis is controlled by cdc25B dephosphorylase activity on Tyr15 and threonine 14 (42). We observed a selective increase in tumor cells that were phosphorylated on Tyr15 of cdc2 when we examined these cells by immunofluorescence (Fig. 4*A*). There was an increase in cytoplasmic distribution of P-Tyr15-p34-cdc2, particularly in the SeMet-treated PC-3 and DU145 prostatic carcinoma cells (Fig. 4*A*). These data are particularly interesting in view of the recent finding that p34-cdc2 is preferentially located in the cytoplasm of human head and neck squamous cell carcinomas (43). In our studies, elevated levels of cdc2 phosphorylation were particularly apparent after SeMet treatment of tumor cell lines. These findings were verified when we examined the phosphorylation status of cdc2 by Western blotting, which revealed a significant increase in P-Tyr15-p34-cdc2 (Fig. 4*C*). There may be a negative regulation of cdc2 phosphorylation involving WEE1 that is influenced by p53. Leach *et al.* (14) reported recently that WEE1 protein kinase may be down-regulated because of p53 activation that resulted in the cumulative dephosphorylation of cdc2, leading to growth arrest and apoptosis. The inactivation of p53 using antisense oligonucleotides, followed by UV irradiation in normal human fibroblasts, was also shown to enhance sensitivity to DNA-damaging agents, implicating p53 in the protection of normal cells. The importance of our findings that selenium can selectively induce G_2-M arrest in prostatic carcinoma by the involvement of cdc2 are highly significant if these events lead to enhanced cell death or potential radiosensitization (44).

Sinha *et al.* (45) reported recently that S-G_2-M phase growth arrest occurred after Na_2SeO_3 treatment and G_1 arrest occurred after MSC treatment in asynchronously dividing mouse mammary epithelial cells (TM6; Ref. 45). These findings are consistent with our results using Na_2SeO_3 in asynchronously dividing prostate cancer cells (PC-3 and DU145). In a second study, these authors established how MSC inhibition affected the timing of the cell cycle by examining synchronized TM6 cells (46). In both studies, they attributed growth inhibition of TM6 cells by MSC to G_1 growth arrest (45, 46). Ip *et al.* (47) also reported that mammary intraductal proliferations induced by methylnitrosourea showed an increase in p27Kip1 (a G_1 checkpoint protein) expression, when rats were fed MSC compared with Na_2SeO_3. In TM6 mammary tumor cells, Na_2SeO_3 preferentially increased cells in S-G_2-M and MSC primarily increased cells arrested in G_1. In human prostate cancer cells, we found that Na_2SeO_3 had greater effects on S-phase than did SeMet but lesser effects on cell arrest in G_2-M. These data demonstrate that different chemical forms of selenium can vary in their effects on the cell cycle and that selenium can act differently in different cell systems.

We observed a decrease in anchorage-independent growth in the presence of SeMet that reflects a potential decrease in tumorigenicity. The high sensitivity of colony formation to SeMet [e.g., SeMet substantially more active in anchorage-independent (Fig. 5) than in monolayer (Fig. 1) PC-3 cells] may involve cell-to-cell interactions related to solid tumor development (48, 49).

The results of our present study are relevant to the molecular mechanisms of selenium actions in prostate carcinogenesis, which are only beginning to be elucidated. Our findings that selenium selectively induces growth inhibition and apoptosis in prostate cancer cells *versus* in prostate normal cells supports the study of selenocompounds for prostate cancer chemoprevention.

Acknowledgments

We thank Dr. Reuben Lotan for contributions to the manuscript. We also thank Norma Llansa and Laura Schaefer for technical support and Kendall Morse for editorial assistance.

References

1. Clark, L. C., Combs, G. F., Jr., Turnbull, B. W., Slate, E. H., Chalker, D. K., Chow, J., Davis, L. S., Glover, R. A., Graham, G. F., Gross, E. G., Krongrad, A., Lesher, J. L., Jr., Park, H. K., Sanders, B. B., Jr., Smith, C. L., and Taylor, J. R. Effects of selenium supplementation for cancer prevention in patients with carcinoma of the skin. A randomized controlled trial. J. Am. Med. Assoc., *276:* 1957–1963, 1996.

2. Clark, L. C., Dalkin, B., Krongrad, A., Combs, G. F., Jr., Turnbull, B. W., Slate, E. H., Witherington, R., Herlong, J. H., Janosko, E., Carpenter, D., Borosso, C., Falk, S., and Rounder, J. Decreased incidence of prostate cancer with selenium supplementation: results of a double-blind cancer prevention trial. Br. J. Urol., *81:* 730–734, 1998.

3. Yoshizawa, K., Willett, W. C., Morris, S. J., Stampfer, M. J., Spiegelman, D., Rimm, E. B., and Giovannucci, E. Study of prediagnostic selenium level in toenails and the risk of advanced prostate cancer. J. Natl. Cancer Inst., *90:* 1219–1224, 1998.

4. Ries, L. A. G., Kosary, C. L., Hankey, B. F., Miller, B. A., and Edwards, B. K. (eds.). SEER Cancer Statistics Review, 1973–1995. Bethesda, MD: National Cancer Institute, 1998.

5. Appel, M. J., and Woutersen, R. A. Effects of dietary β-carotene and selenium on initiation and promotion of pancreatic carcinogenesis in azaserine-treated rats. Carcinogenesis (Lond.), *17:* 1411–1416, 1996.

6. van Lieshout, E. M. M., Ekkel, M. P. C., Bedaf, M. M. G., Nijhoff, W. A., and Peters, W. H. M. Effects of dietary anticarcinogens on rat gastrointestinal glutathione peroxidase activity. Oncol. Rep., *5:* 959–963, 1998.

7. Zhang, Z., Kimura, M., and Itokawa, Y. The decrement of carcinogenesis by dietary selenium and expression of placental form of glutathione-*S*-transferase in rat glioma. Biol. Trace Elem. Res., *57:* 147–155, 1997.

8. Ip, C. Lessons from basic research in selenium and cancer prevention. J. Nutr., *128:* 1845–1854, 1998.

9. Furr, A. K., Parkinson, T. F., Bache, C. A., Gutenmann, W. H., Pakkala, I. S., and Lisk, D. J. Elemental content of vegetables and millet grown in potted soil amended with lignite fly ash. Arch. Environ. Contam. Toxicol., *10:* 647–651, 1981.

10. Kadrabova, J., Madaric, A., Kovacikova, Z., and Ginter, E. Selenium status, plasma zinc, copper, and magnesium in vegetarians. Biol. Trace Elem. Res., *50:* 13–24, 1995.

11. Daniels, L. A. Selenium metabolism and bioavailability. Biol. Trace Elem. Res., *54:* 185–199, 1996.

12. Prasad, S. C., Soldatenkov, V., Notario, V., Smulson, M., and Dritschilo, A. Detection of heterogeneity of apoptotic fragments of poly (ADP-ribose) poly-

merase in MDA-MB-468 breast cancer cells: two-dimensional gel analysis. Electrophoresis, *20:* 618–625, 1999.

13. Furnari, B., Blasina, A., Boddy, M. N., McGowan, C. H., and Russell, P. Cdc25 inhibited *in vivo* and *in vitro* by checkpoint kinases Cds1 and Chk1. Mol. Biol. Cell, *10:* 833–845, 1999.

14. Leach, S. D., Scatena, C. D., Keefer, C. J., Goodman, H. A., Song, S. Y., Yang, L., and Pietenpol, J. A. Negative regulation of Wee1 expression and Cdc2 phosphorylation during p53-mediated growth arrest and apoptosis. Cancer Res., *58:* 3231–3236, 1998.

15. Fujiwara, N., Fujii, T., Fujii, J., and Taniguchi, N. Functional expression of rat thioredoxin reductase: selenocysteine insertion sequence element is essential for the active enzyme. Biochem. J., *340:* 439–444, 1999.

16. Wingler, K., Bocher, M., Flohe, L., Kollmus, H., and Brigelius-Flohe, R. mRNA stability and selenocysteine insertion sequence efficiency rank gastrointestinal glutathione peroxidase high in the hierarchy of selenoproteins. Eur. J. Biochem., *259:* 149–157, 1999.

17. Gasdaska, P. Y., Berggren, M. M., Berry, M. J., and Powis, G. Cloning, sequencing and functional expression of a novel human thioredoxin reductase. FEBS Lett., *442:* 105–111, 1999.

18. Shen, H. M., Yang, C. F., and Ong, C. N. Sodium selenite-induced oxidative stress and apoptosis in human hepatoma HepG2 cells. Int. J. Cancer, *81:* 820–828, 1999.

19. Yan, L., and Spallholz, J. E. Generation of reactive oxygen species from the reaction of selenium compounds with thiols and mammary tumor cells. Biochem. Pharmacol., *45:* 429–437, 1993.

20. Brtko, J., Filipcik, P., Hudecova, S., Brtkova, A., and Bransova, J. Nuclear all-*trans* retinoic acid receptors: *in vitro* effects of selenium. Biol. Trace Elem. Res., *62:* 43–50, 1998.

21. Stewart, M. S., Spallholz, J. E., Neldner, K. H., and Pence, B. C. Selenium compounds have disparate abilities to impose oxidative stress and induce apoptosis. Free Radical Biol. Med., *26:* 42–48, 1999.

22. Kajander, E. O., Harvima, R. J., Kauppinen, L., Akerman, K. K., Martikainen, H., Pajula, R. L., and Karenlampi, S. O. Effects of selenomethionine on cell growth and on *S*-adenosylmethionine metabolism in cultured malignant cells. Biochem. J., *267:* 767–774, 1990.

23. Redman, C., Scott, J. A., Baines, A. T., Basye, J. L., Clark, L. C., Calley, C., Roe, D., Payne, C. M., and Nelson, M. A. Inhibitory effect of selenomethionine on the growth of three selected human tumor cell lines. Cancer Lett., *125:* 103–110, 1998.

24. Ganther, H. E. Selenium metabolism, selenoproteins and mechanisms of cancer prevention: complexities with thioredoxin reductase. Carcinogenesis (Lond.), *20:* 1657–1666, 1999.

25. Ip, C., Thompson, H. J., Zhu, Z., and Ganther, H. E. *In vitro* and *in vivo* studies of methylseleninic acid: evidence that a monomethylated selenium metabolite is critical for cancer chemoprevention. Cancer Res., *60:* 2882–2886, 2000.

26. Tang, D. G., Li, L., Chopra, D. P., and Porter, A. T. Extended survivability of prostate cancer cells in the absence of trophic factors: increased proliferation, evasion of apoptosis, and the role of apoptosis proteins. Cancer Res., *58:* 3466–3479, 1998.

27. Althaus, F. R., Kleczkowska, H. E., Malanga, M., Muntener, C. R., Pleschke, J. M., Ebner, M., and Auer, B. Poly ADP-ribosylation. a DNA break signal mechanism. Mol. Cell. Biochem., *193:* 5–11, 1999.

28. Pieper, A. A., Verma, A., Zhang, J., and Snyder, S. H. Poly(ADP-ribose) polymerase, nitric oxide and cell death. Trends Pharmacol. Sci., *20:* 171–181, 1999.

29. Guenette, R. S., Daehlin, L., Mooibroek, M., Wong, K., and Tenniswood, M. Thanatogen expression during involution of the rat ventral prostate after castration. J. Androl., *15:* 200–211, 1994.

30. Simbulan-Rosenthal, C. M., Rosenthal, D. S., Iyer, S., Boulares, H., and Smulson, M. E. Involvement of PARP and poly(ADP-ribosyl)ation in the early stages of apoptosis and DNA replication. Mol. Cell. Biochem., *193:* 137–148, 1999.

31. Simbulan-Rosenthal, C. M., Rosenthal, D. S., Iyer, S., Boulares, A. H., and Smulson, M. E. Transient poly(ADP-ribosyl)ation of nuclear proteins and role of poly(ADP-ribose) polymerase in the early stages of apoptosis. J. Biol. Chem., *273:* 13703–13712, 1998.

32. Boulares, A. H., Yakovlev, A. G., Ivanova, V., Stoica, B. A., Wang, G., Iyer, S., and Smulson, M. Role of poly(ADP-ribose) polymerase (PARP) cleavage in apoptosis. Caspase 3-resistant PARP mutant increases rates of apoptosis in transfected cells. J. Biol. Chem., *274:* 22932–22940, 1999.

33. Hofmann, E. R., Boyanapalli, M., Lindner, D. J., Weihua, X., Hassel, B. A., Jagus, R., Gutierrez, P. L., Kalvakolanu, D. V., and Hofman, E. R. Thioredoxin reductase mediates cell death effects of the combination of beta interferon and retinoic acid. Mol. Cell. Biol., *18:* 6493–6504, 1998.

34. Lindner, D. J., Hofmann, E. R., Karra, S., and Kalvakolanu, D. V. The interferon-β and tamoxifen combination induces apoptosis using thioredoxin reductase. Biochim. Biophys. Acta, *1496:* 196–206, 2000.

35. Smulson, M. E., Pang, D., Jung, M., Dimtchev, A., Chasovskikh, S., Spoonde, A., Simbulan-Rosenthal, C., Rosenthal, D., Yakovlev, A., and Dritschilo, A. Irreversible binding of poly(ADP)ribose polymerase cleavage product to DNA ends revealed by atomic force microscopy: possible role in apoptosis. Cancer Res., *58:* 3495–3498, 1998.

36. Fraker, P. J., King, L. E., Lill-Elghanian, D., and Telford, W. G. Quantification of apoptotic events in pure and heterogeneous populations of cells using the flow cytometer. Methods Cell Biol., *46:* 57–76, 1995.

37. Cejna, M., Fritsch, G., Printz, D., Schulte-Hermann, R., and Bursch, W. Kinetics of apoptosis and secondary necrosis in cultured rat thymocytes and S.49 mouse lymphoma and CEM human leukemia cells. Biochem. Cell Biol., *72:* 677–685, 1994.

38. Blank, R. S., Thompson, M. M., and Owens, G. K. Cell cycle *versus* density dependence of smooth muscle α actin expression in cultured rat aortic smooth muscle cells. J. Cell Biol., *107:* 299–306, 1988.

39. Bijur, G. N., Briggs, B., Hitchcock, C. L., and Williams, M. V. Ascorbic acid-dehydroascorbate induces cell cycle arrest at G2/M DNA damage checkpoint during oxidative stress. Environ. Mol. Mutagen, *33:* 144–152, 1999.

40. Bernhard, E. J., Maity, A., Muschel, R. J., and McKenna, W. G. Effects of ionizing radiation on cell cycle progression. A review. Radiat. Environ. Biophys., *34:* 79–83, 1995.

41. Jin, P., Hardy, S., and Morgan, D. O. Nuclear localization of cyclin B1 controls mitotic entry after DNA damage. J. Cell Biol., *141:* 875–885, 1998.

42. Lammer, C., Wagerer, S., Saffrich, R., Mertens, D., Ansorge, W., and Hoffmann, I. The cdc25B phosphatase is essential for the G2/M phase transition in human cells. J. Cell Sci., *111:* 2445–2453, 1998.

43. Cohen-Jonathan, E., Toulas, C., Rochaix, P., Bachaud, J. M., Daly-Schveitzer, N., and Favre, G. Preferential cytoplasmic localization of p34cdc2 in recurrent human squamous cell carcinoma after radiotherapy. Radiat. Res., *147:* 277–283, 1997.

44. Kyprianou, N., Bains, A., and Rhee, J. G. Transient tyrosine phosphorylation of p34cdc2 is an early event in radiation-induced apoptosis of prostate cancer cells. Prostate, *32:* 266–271, 1997.

45. Sinha, R., Said, T. K., and Medina, D. Organic and inorganic selenium compounds inhibit mouse mammary cell growth *in vitro* by different cellular pathways. Cancer Lett., *107:* 277–284, 1996.

46. Sinha, R., and Medina, D. Inhibition of cdk2 kinase activity by methylselenocysteine in synchronized mouse mammary epithelial tumor cells. Carcinogenesis (Lond.), *18:* 1541–1547, 1997.

47. Ip, C., Thompson, H. J., and Ganther, H. E. Selenium modulation of cell proliferation and cell cycle biomarkers in normal and premalignant cells of the rat mammary gland. Cancer Epidemiol. Biomark. Prev., *9:* 49–54, 2000.

48. Orford, K., Orford, C. C., and Byers, S. W. Exogenous expression of β-catenin regulates contact inhibition, anchorage-independent growth, anoikis, and radiation-induced cell cycle arrest. J. Cell Biol., *146:* 855–868, 1999.

49. Kantak, S. S., and Kramer, R. H. E-cadherin regulates anchorage-independent growth and survival in oral squamous cell carcinoma cells. J. Biol. Chem., *273:* 16953–16961, 1998.